

LASER GYROSCOPE BASED ON SYNCHRONOUSLY PUMPED BIDIRECTIONAL
FIBER OPTICAL PARAMETRIC OSCILLATOR

By

Jeffrey Noble

Copyright © Jeffrey Scott Noble 2017

A Thesis Submitted to the Faculty of the

COLLEGE OF OPTICAL SCIENCES

In Partial Fulfillment of the Requirements

For the Degree of

MASTERS OF SCIENCE

In the Graduate College

THE UNIVERSITY OF ARIZONA

2017

STATEMENT BY AUTHOR

The thesis titled ‘Laser Gyroscope based on Synchronously Pumped Bidirectional Fiber Optical Parametric Oscillator’ prepared by Jeffrey Noble has been submitted in partial fulfillment of requirements for a master’s degree at the University of Arizona and is deposited in the University Library to be made available to borrowers under rules of the Library.

Brief quotations from this thesis are allowable without special permission, provided that an accurate acknowledgement of the source is made. Requests for permission for extended quotation from or reproduction of this manuscript in whole or in part may be granted by the head of the major department or the Dean of the Graduate College when in his or her judgment the proposed use of the material is in the interests of scholarship. In all other instances, however, permission must be obtained from the author.

SIGNED: *Jeffrey Noble*

APPROVAL BY THESIS DIRECTOR

This thesis has been approved on the date shown below:

<hr/>	<u>5/22/17</u>
<i>Khanh Kieu</i>	Date
<i>Assistant Professor of Optical Sciences</i>	

Acknowledgement

First, I would like to thank Dr. Khanh Kieu for advising me during my time as a graduate student at the University of Arizona. It was only with his help and guidance I could complete this project. Dr. Kieu was always willing to help with tests experiments in lab while inciting knowledge that expanded my understand of the subjects that were needed to complete this program. I would also like to thank everyone that I worked in the Ultrafast Fiber Lasers and Nonlinear Optics Group. It was always a pleasure working alongside all of them during my time at the University.

Next, I would like to thank Chase and Lauren Salsbury. Without their support, I would not have been able to make it through the master's program or the undergrad program. Finally, thank you to my family. Always being there with encouraging words, love and support. Thank you.

TABLE OF CONTENTS

List of Figures	5
Abstract	7
1) Introduction	8
1.1 Sagnac Effect	8
1.2 Ring Laser Gyroscope.....	10
1.3 Lock In Bias and Dither	11
1.4 Fiber Optic Gyroscope	12
1.5 Polarization and Fiber Optics.....	14
1.6 Fiber Optical Parametric Oscillator	17
1.7 Mode-Locked Laser Gyroscope.....	20
2) Experimental Design	23
2.1 Mode Lock Laser Design	24
2.2 Bidirectional Fiber Optical Parametric Oscillator Design	30
2.3 Housing Design.....	31
3) Results	34
4) Conclusion	43
References.....	44

List of Figures

Figure 1.1 Basic Sagnac Effect Example	8
Figure 1.2 Shows that a triangle shape (as well as others) can used for a closed loop interferometer.....	9
Figure 1.3 Left: Ring Laser Gyroscope Right: Better image of an active ring laser gyroscope. These two show that the cavity can be constructed in multiple shapes [6], [7].....	10
Figure 1.4 Interferometric Fiber Optic Gyroscope [9]	12
Figure 1.5 Resonant Fiber Optic Gyroscope [12]	13
Figure 1.6 Different Cladding and Core designs for optical fibers. [14].....	15
Figure 1.7 Shows the attenuation in silica fibers over a range of wavelengths. [14].....	16
Figure 1.8 The three most common designs of polarization maintaining fiber [18]	17
Figure 1.9 To the left is schematic for a bulk, free-space optical parametric oscillator. The image on the right shows a simple plot of the input and output of an OPO [RP Photonics]	18
Figure 1.10 An experimental design for a bidirectional, synchronously pump, ring optical parametric oscillator [20]	18
Figure 1. 11 Normal Dispersion FOPO [21]	19
Figure 1.12 a) Degenerate FWM in the frequency domain b) Non-degenerate FWM in the frequency domain c) Degenerate FWM in an energy level diagram d) Non-degenerate FWM in an energy level diagram [22].....	20
Figure 2.1 Schematic of the experiment consisting of the mode locked laser pump, fiber amplifier, and a bidirectional OPO	23
Figure 2.2 Schematic of Mode-Lock Fiber Laser	24
Figure 2.3 Setup for testing polarization, and the resulting voltage outputs.....	25
Figure 2.4 Mode-Locked Laser's output power	25
Figure 2.5 Multiple OSA readings for output spectrum of the Mode-Locked Laser.....	26
Figure 2.6 Top: Oscilloscope Reading Bottom: Autocorrelation of the Mode-Locked Laser.....	27

Figure 2.7 Isolator and Erbium Doped Fiber Amplifier	28
Figure 2.8 Output power after the amplifier. The pump current for the Mode-Locked laser remained constant while the pump for the amplifier was adjusted.	28
Figure 2.9 OSA readings after the amplifier.....	29
Figure 2.10 Couplers and Bidirectional Optical Parametric Oscillator.....	30
Figure 2.11 Layout in the bottom layer of foam	32
Figure 2.12 CAD drawing of the housing with the material components	32
Figure 3.1 OSA reading for both arms and the recombined signal.....	35
Figure 3.2 Left: shows the beatnote around the Repetition Rate. Right is a closer look at the beatnote signal	36
Figure 3.3 Time Signal and Fourier Transform.....	37
Figure 3.4 Frequency Counter readings with and without the foam	38
Figure 3.5 Power Readings from both arms	38
Figure 3.6 A zoomed in image of the power readings	39
Figure 3.7 Shows the location of both the temperature probes in the system	40
Figure 3.8 The relationship between temperature (top) and the frequency change/drift (bottom).....	41
Figure 3.9 Fourier Transform of the drift measurements. Right is a zoomed in view of the left plot.....	41

Abstract

This master thesis presents an experimental design of a laser gyroscope based on a stabilized fiber optical parametric oscillator frequency comb and the results of testing of the proposed design. Before going into the experimental details, a background for different types of gyroscopes is discussed. This new laser gyroscope design is made up of only polarization maintaining (PM) fiber and PM fiber components. By using only fiber and fiber components, we were able to minimize size, weight, and alignment issues that are typical in bulk optical designs for OPO's and gyroscopes.

The fiber-based OPO produces counter propagating ultrafast pulses that overlap only twice in the cavity, resulting in a beatnote signal when combined outside of the laser cavity. A mode-locked laser is used as a pump source so the lock-in effect (or deadband region) is avoided for the experiment. The drift of this beatnote signal represents the rotation sensitivity of the experimental setup. Issues seen in past iterations, such as stability of mode-locked pump source and beatnote drift overtime due to environmental variables, have been reduced in this experiment. This has been done by comprising the entire pump source of PM components, and by placing the entire setup in an insulating box to minimize acoustic and temperature fluctuations. By creating a frequency comb and locking the laser gyroscope to an optical clock, this experiment can be used for very precise rotation sensing in comparison to other gyro designs currently available.

1) Introduction

1.1 Sagnac Effect

In 1913, Georges Sagnac first experimentally proved the “Sagnac Effect” by showing the correlation between the angular velocity and fringe phase-shift in a ring interferometer of a defined area [1]. In a rotating system, two beams of light were propagated in opposing directions resulting in two different round trip times and different path lengths. From this result, he derived two basic equations:

$$\delta t = \frac{4\Omega \cdot A}{v^2}; \delta\phi = \frac{8\pi\Omega \cdot A}{\lambda v} \tag{1.1}$$

Where δt is the difference in round trip time, Ω is the angular rate of rotation, A is the area of the ring interferometer, and v is the velocity of the beam. In the second equation $\delta\phi$ is the relative phase shift and λ is the wavelength of the beam [1]. A basic example for the Sagnac Effect is to picture a disk spinning in a counter clockwise manner. If two optical signals are propagating, one clockwise and counterclockwise, the signal that is traveling with the rotation (in this case the counter clockwise signal) will take longer time to travel completely around the disk compared to the other signal that is traveling against the rotation direction. In figure 1.1 this phenomenon is shown.

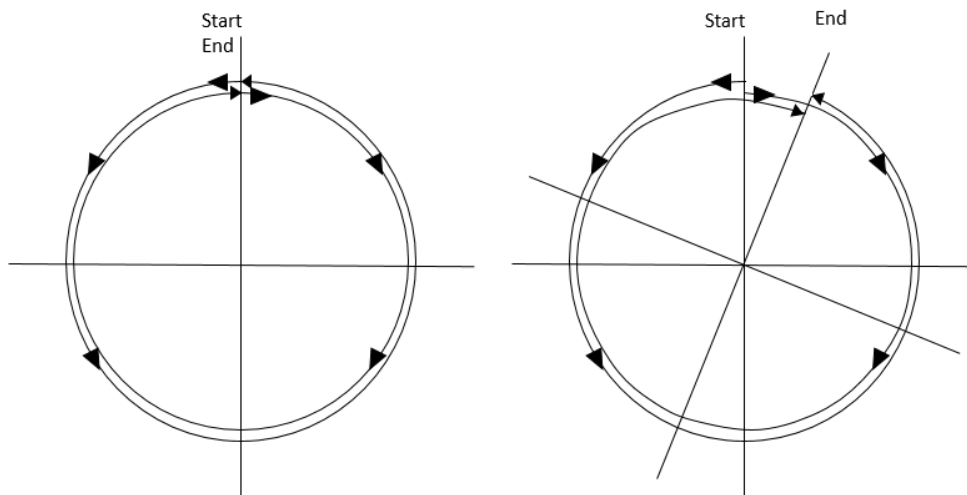


Figure 1.1 Basic Sagnac Effect Example

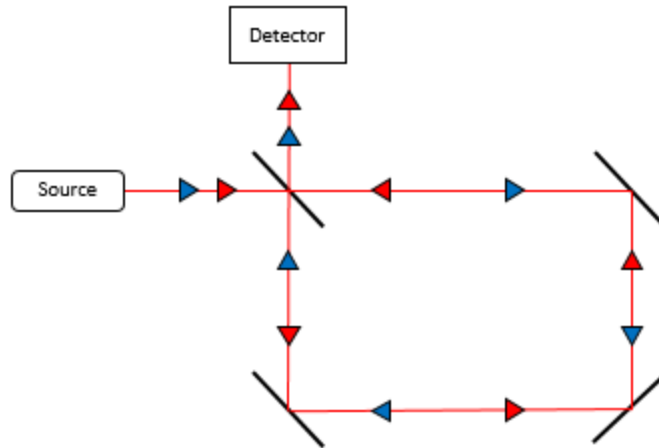


Figure 1.2 Shows that a triangle shape (as well as others) can be used for a closed loop interferometer

When thinking of rotating, the initial thought might be of using a circular design, but this effect can be shown for any shape with a closed path. Here is a setup for a construction proposed by Michelson. If a closed loop is constructed with a beam splitter, a square mirror cavity, the Sagnac effect can still be seen on the detector, if everything including the source and detector are rotated as well [2].

This Sagnac effect has been observed in multiple interferometric setups. The first implementation is a passive setup, this is when an outside light source is counter propagated, and a phase shift is measured from the interference of the counter-propagating beams resulting in a fringe pattern that is observed outside of the cavity [2]. The second implementation, which is currently used for inertial guidance systems, is the active Sagnac interferometer. In this set up the phase shift is converted into a frequency shift between the two propagating laser beams [3]. The loop is closed, creating a laser cavity, which results in converting the phase shift into a frequency shift. This difference in frequency can be represented by:

$$\Delta f = \frac{4A \cdot \Omega}{\lambda P} \quad (1.2)$$

Where Δf is the difference in frequency, Ω is rotation rate, and P is the perimeter of the closed loop. For example, if a ring is being used with a radius of 1m, a laser wavelength of 632.3nm, and a beatnote frequency of 1Hz (which can be easily measured), the rotation rate is shown in the equation below.

$$\Delta f = \frac{4\Omega\pi R^2}{\lambda 2\pi R} = \frac{2\Omega R}{\lambda}$$

$$\Omega = \frac{\Delta f \lambda}{2R} = \frac{1\text{Hz} * 632.3\text{nm}}{2 * 1\text{m}}$$

$$\Omega = 1.99 * 10^{-6} \text{ rad/s}$$

For reference the earth rotates at:

$$\Omega_{earth} = 7.29 * 10^{-5} \text{ rad/s}.$$

A downside to the active interferometric setup, there is a chance of a lock-in effect, which will be discussed in future sections.

1.2 Ring Laser Gyroscope

One of the most popular devices that uses the Sagnac effect is the ring laser gyro. Typically, the orientation of the ring laser gyro is a square or rectangle, shown in the figure below [4]. The cavity is created by using multiple mirrors and a beam splitter or a small partially transmitting mirror to extract the signal to be observed on a detector. Inside the cavity, a lasing medium is introduced to create an active ring resonator [5].

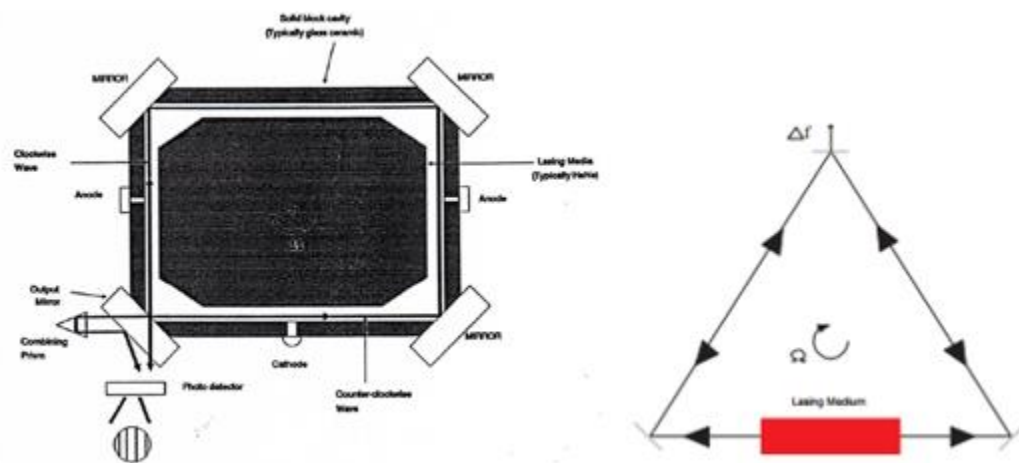


Figure 1.3 Left: Ring Laser Gyroscope Right: Better image of an active ring laser gyroscope. These two show that the cavity can be constructed in multiple shapes [6], [7]

The difference in frequency for both paths are dependent on the total area that the ring encompasses and the rotation velocity. The interference pattern is dependent on this change in frequency, or beat frequency, and can be stated as [6] :

$$I = I_o(1 + \cos(2\pi\Delta ft)) \quad (1.5)$$

This technique can produce high performance results. It offers high sensitivity and stability, quick reaction time, insensitivity to acceleration and most environmental effects. Even with these advantages over the mechanical gyros, the ring laser gyro is a difficult device to produce. The size, weight, and cost of these devices are a very significant issue. Other issues with them are the sensitivity of electromagnetic interference, lifetime, and lock-in effect when small/slow rotations are present [7]. As previously stated, the frequency detected is based off the area of the gyro so many of the past experiments have been done by increasing the size to measure the most precise frequency shift that is possible. Unfortunately when the cavity increases in size it is more difficult to keep a stable resonator [7]. By moving to a fiber-based design the size/weight of the device can decrease drastically, and the sensitivity can potentially be increased.

1.3 Lock In Bias and Dither

In the ring laser gyro a major issue is the lock-in effect at lower rotation rates. When this scenario occurs the optical frequency of two counter propagating beams lock to one another resulting in no beat frequency. The range of frequencies where this can occur is known as the dead band region [6]. In a ring laser gyro typically a continuous wave laser is used, this results in the counter-propagating optical fields interacting (through backscattering) constantly in multiple locations in the cavity. This continuous-wave (CW) operation is where the lock in effect becomes a real issue. By replacing the CW source with a mode locked laser the interaction area is minimized to two locations, and thus can mitigate the lock in issue. A common technique that can be used to avoid this lock in region is by mechanical dithering. By using this approach noise is intentionally added to the system. This can be done mechanically by rotating the gyro through very small angles at a rapid rate, and the lock in will only occur when the rotation velocity is at or near zero. The error, in theory, will be cancelled between dead periods.

Other ways that dithering can be performed is by adding a bias beatnote through phase modulation of the propagating beams. A very practical approach to this technique is to apply

equal, and opposite bias to each direction that periodically will reverse direction. By doing so this will lead to an average over all time that will equal to zero [2]. The net result is that only the beat frequency is measured.

A bias beat note is defined as the frequency difference reading that is not from a rotation. A bias beatnote, that was not intentionally introduced, can be induced through multiple factors, such as environmental fluctuations, electromagnetic fields, and nonlinear optical effects [2].

1.4 Fiber Optic Gyroscope

There are two different types of fiber gyros that are currently being used/ under development. The interferometric fiber optic gyroscope (IFOG) and the resonant fiber optic gyroscope (RFOG). The IFOG is currently considered the more main stream option, but the RFOG has shown more potential for future use [7]. The interferometric fiber optic gyro uses fringe pattern shift from the Sagnac Effect to measure rotation while the resonator fiber optic gyro uses a resonant fiber cavity to measure rotation rate based on the Sagnac Effect. Similar to what was stated earlier, the phase difference between the counter propagating beams is

$$\Delta\Phi = \frac{2\pi LD}{\lambda c} \quad (1.6)$$

Where the length of the fiber is defined as: $L = N\pi D$. In the figure shown is a simple configuration of an IFOG [8].

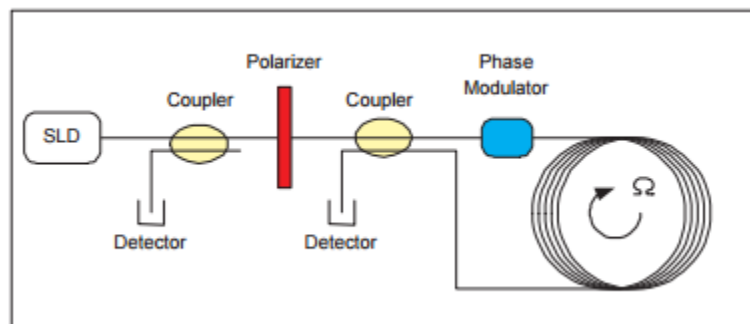


Figure 1.4 Interferometric Fiber Optic Gyroscope [9]

In the IFOG set up, a low coherence light source should be used in order to minimize some noise in the system [9]. A polarizer is placed in the design in order to remove polarization delay of the two propagating beams. Next two couplers and detectors are used because the transmission and

coupling characteristics of a coupler are not equal. Both of the propagating waves need to experience these factors in an identical way [10]. Finally, a phase modulator is used to induce a π halves bias phase difference so a better sensitivity of the measurements can be observed.

The rotation velocity is considered to be the driving force behind the operating range of the IFOG. This value can be defined as [11]:

$$\Omega_{\pi} = \frac{\lambda c}{2LD} \quad (1.7)$$

So, by considering this equation, the two degrees of freedom that are easier to adjust the operating range of the IFOG are the length of the fiber and the diameter of the coil used. The issues in the IFOG come from numerous noise factors, the Kerr effect, and thermal variations [8].

The second fiber gyro is the resonant type. This setup is more similar to the ring laser gyroscope due to the fact that it needs a laser source with narrow emission bandwidth and uses an optical cavity to excite a single cavity mode that is supported by the fiber coil. This is considered a passive resonator approach because there is no gain medium in the coil [7].

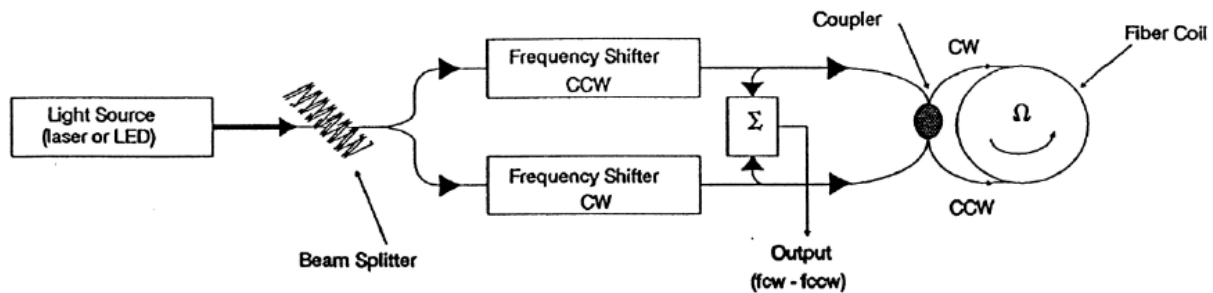


Figure 1.5 Resonant Fiber Optic Gyroscope [12]

In this design, a resonator is constructed by using a beam splitter and some amount of optical fiber. Normally the RFOG does not need a large amount of fiber like the IFOG. Each counter propagating beam has a frequency shifter in order to observe the resonant frequency of both the clockwise and counter clockwise beams due to the Sagnac effect. The beat frequency cannot be measured directly within the resonator in this design. Once this device is rotated one of the beams paths will become shorter resulting in a frequency shift, and a difference in frequency

between the CW and the CCW, consequently resulting in a split in resonant frequency. Similar to the IFOG, the RFOG has issues with the same limitations, but has a higher upside when it comes to sensitivity. When using less fiber in the system, it can mitigate some of the environmental issues such as thermal variation. Another tradeoff between the two can be the fact that if less fiber is being used in the design it would reduce cost, but most of the RFOG designs have to use polarization maintaining fiber which can be much more expensive than standard single mode fiber [7].

1.5 Polarization and Fiber Optics

Optical fiber is a very popular medium to use as a waveguide due to its low propagation loss. When using an all fiber system instead of a bulk optical system (lens, mirrors, etc.) issues such as, alignment, size, and sensitivity can be controlled/ mitigated in order to have a more robust design. The standard design of an optical fiber is to have a higher refractive index in the core, with a lower refractive index in the cladding to induce total internal reflection so light will travel down the fiber with low loss [13]. Figure 1.3 shows three common layouts of optical fibers, and how the light travels through them. For the purpose of this project a variation of the single mode fiber will be used. In order for the fiber to operate with only one mode the V number of the fiber must be below a value of 2.405 [13]. The V number depends on the radius of the core of the fiber, the wavelength of the light sent into the fiber, and the numerical aperture. The equation showing the relationship of these variables is:

$$V = \frac{2\pi}{\lambda} aNA = \frac{2\pi}{\lambda} a \sqrt{n_{core}^2 - n_{cladding}^2}. \quad (1.3)$$

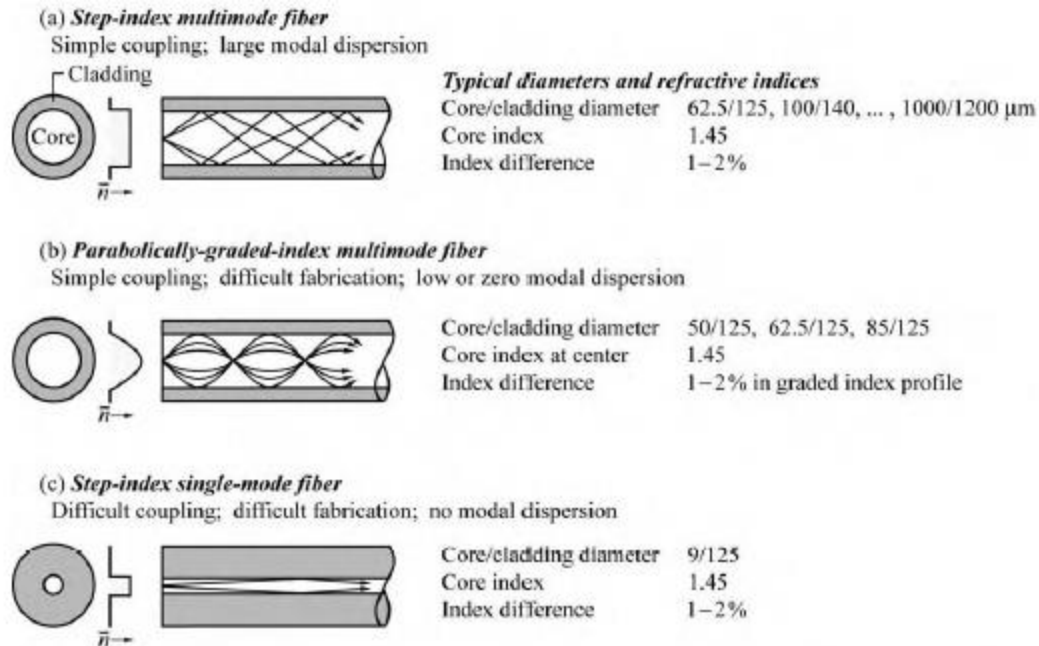


Figure 1.6 Different Cladding and Core designs for optical fibers. [14]

Optical fiber has very small amounts of propagation loss, especially in single mode silica fibers. The loss in these particular fibers is mostly dominated by, different scattering phenomena, such as Rayleigh, Brillouin, and Raman. Rayleigh scattering occurs normally at shorter wavelengths, and is the result of the variation of the refractive index of the glass. Brillouin scattering is considered a nonlinear effect, and occurs when a photon is converted into a backward propagating scattered photon of lower energy and an acoustic phonon [15]. The last scattering mentioned is Raman scattering. This is also considered a nonlinear effect. Raman scattering occurs when the propagating light's intensity triggers a nonlinear response from the chemical bounds, the bond between the silicon atom and oxygen atom in case of fused silica glass [16]. The propagation loss for silica fibers can reach a minimum of about 0.2db/km, and this occurs in the range of 1550nm-1600nm. For this reason, the majority of optical telecommunications, and other optical fiber components work in this wavelength range [13], [14].

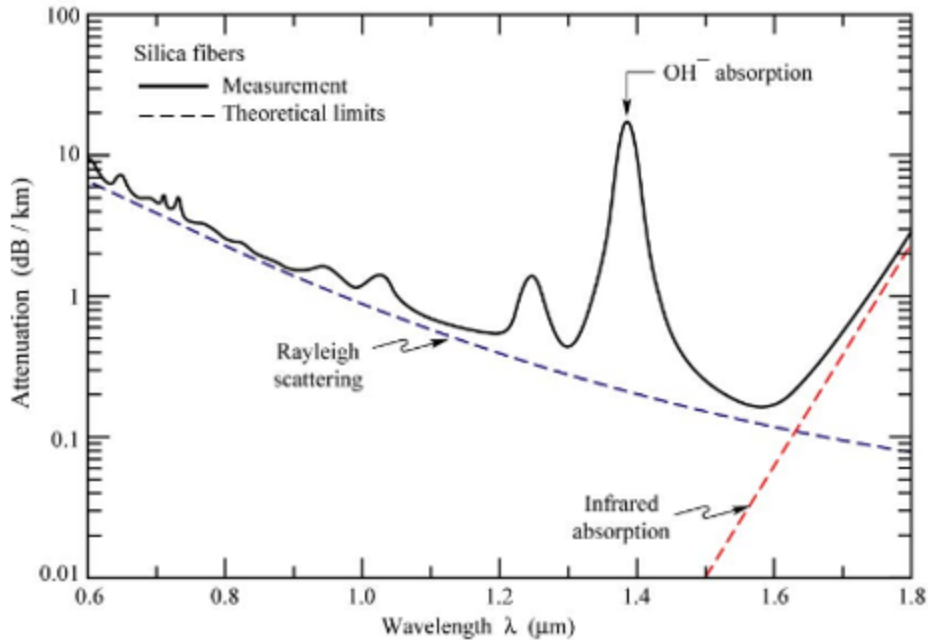


Figure 1.7 shows the attenuation in silica fibers over a range of wavelengths. [14]

All optical fibers have some birefringence, due to some amount of mechanical stress, or some natural deformities in the symmetry of the wave guide. Birefringence is a phenomenon in which the refractive index is dependent on the polarization direction. This is an issue because the light can have different phase velocities depending on which polarization state it is associated with at any given time [13], [17]. Subsequently, the light can propagate at different speeds through the fiber, and change polarization once exiting the fiber. This issue is resolved by using polarization-maintaining fiber. Counter-intuitively, this type of fiber does not remove the birefringence, but creates a very strong birefringence in order to control the polarization. The light that is launched in can be aligned to one of the birefringent axes resulting in the preservation of the polarization state through the entire wave guide [18]. The figure below shows how the design of the fiber changes so the birefringence is increased to a strong level.

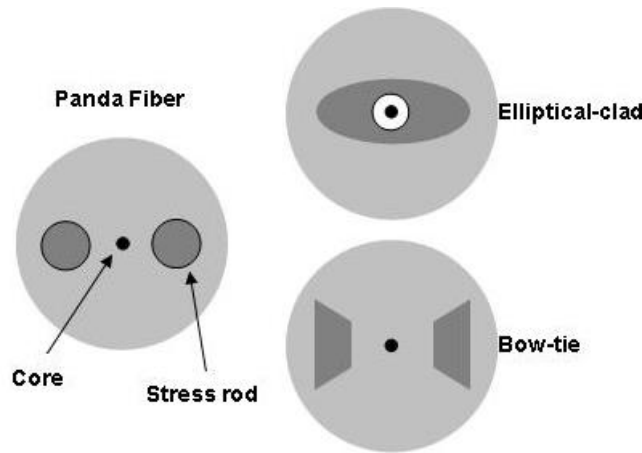


Figure 1.8 The three most common designs of polarization maintaining fiber [18]

The first technique is by adding stress rods that go along the fiber's core. This is seen in the most left fiber also known as panda fiber. Two cylindrical rods are added, one on each side of the core to create mechanical stress with a well-defined orientation. The bottom right design, known as the bow-tie fiber, works in a similar way, however the stress rods are not in a cylindrical shape. [18] The final design is the top right which instead of adding stress rods, creates an elliptical core, which without adding any additional mechanical stress forms a clear orientation for the birefringence. [17] Using polarization-maintaining fiber has its pros and cons, just like everything else. One positive feature, which for this project is a very important reason, is outside variables will not have as much effect on the signal's polarization state, such as fiber bending and temperature changes. The signal/polarization state should stay very steady through the PM fiber. A disadvantage of this type of fiber is that if the alignment of components/fiber is not perfect. A very large amount of loss can be induced into the system.

1.6 Fiber Optical Parametric Oscillator

The optical parametric oscillator is a source that is related to a laser/laser resonator, but instead of using stimulated emission, the optical gain is from parametric amplification in a nonlinear crystal/medium. This is an attractive device because it has the ability to obtain radiation in different wavelength regions with high conversion efficiencies [19]. An OPO can produce the signal and idler wavelengths through the phase-matching condition within a very large range of wavelengths. This gives the capability to access wavelengths that cannot be obtained by some

standard lasers [19]. Below is the schematic of a bulk optical parametric oscillator, and a plot of the input and output of the device.

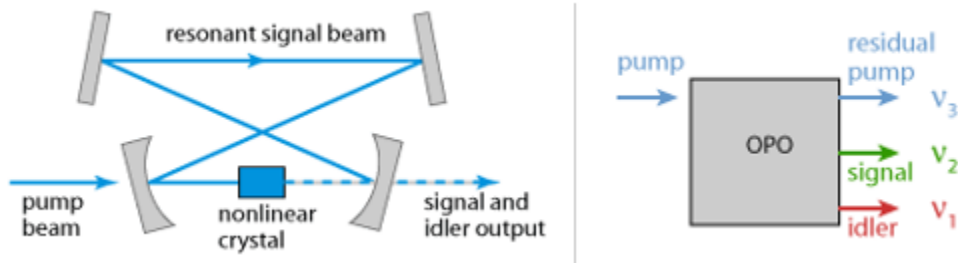


Figure 1.9 To the left is schematic for a bulk, free-space optical parametric oscillator. The image on the right shows a simple plot of the input and output of an OPO [RP Photonics]

A specific bulk OPO that is relatable for this project is a bidirectional, synchronously pumped, ring optical parametric oscillator. This experiment uses a mode locked Ti-Sapphire laser as the pump source working at 790nm, and a periodically poled LiNbO₃ crystal is used in the OPO. A signal of 1.4um is produced in the OPO. Due to bulk optics being used for the cavity, the sensing area is limited [20].

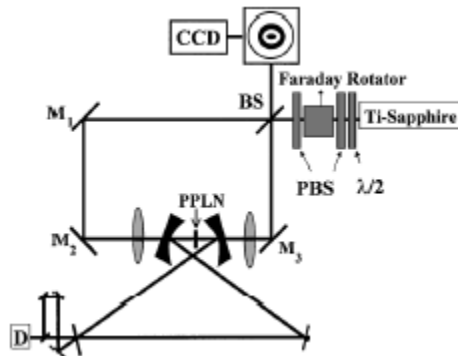


Figure 1.10 An experimental design for a bidirectional, synchronously pump, ring optical parametric oscillator [20]

Bulk optics can be expensive, very sensitive to adjustment of the optical elements, and can only convert radiation to longer wavelengths. This OPO is possible in solid state gyroscopes by a technique of three wave mixing. This interaction of three waves is from the second order non-linear induced polarization [20].

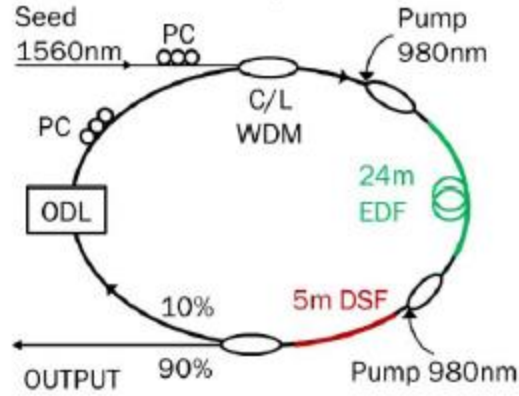


Figure 1. 11 Normal Dispersion FOPO [21]

An alternative to this, which will benefit this project, is using a fiber optical parametric oscillator based on four wave mixing. In the four-wave mixing scenario, the second order non-linear components are zero due to symmetry so four wave mixing occurs because of the third order non-linearity [22]. The positives in using a FOPO are: a large range of phase matching and tuning; good beam quality; weight and compactness; and stability. Similar to the bulk OPO, the fiber optical parametric oscillator has to meet the phase matching criteria, but also satisfy the conservation of momentum and energy. Below is the equation for conservation of momentum where k is wave number, β is propagation constant, ω is frequency, and n is index [19].

$$\Delta k_M = \beta_4 + \beta_3 - \beta_1 - \beta_2 = 0 = \frac{n_4\omega_4 + n_3\omega_3 - n_1\omega_1 - n_2\omega_2}{c} \quad (1.4)$$

The four-wave mixing (FWM) process occurs when two pump photons generate two new waves; the signal and idler waves. There are two different scenarios of when the pump photons are the same (degenerate FWM) or when two different pump wavelengths are contributing [22]. Figure 1.8 shows how the frequencies relate to one another in both cases. Following that is another schematic showing the conservation of energy using different levels, where ω_1 and ω_2 are the pump wavelengths and ω_3 and ω_4 are the signal and idler [22].

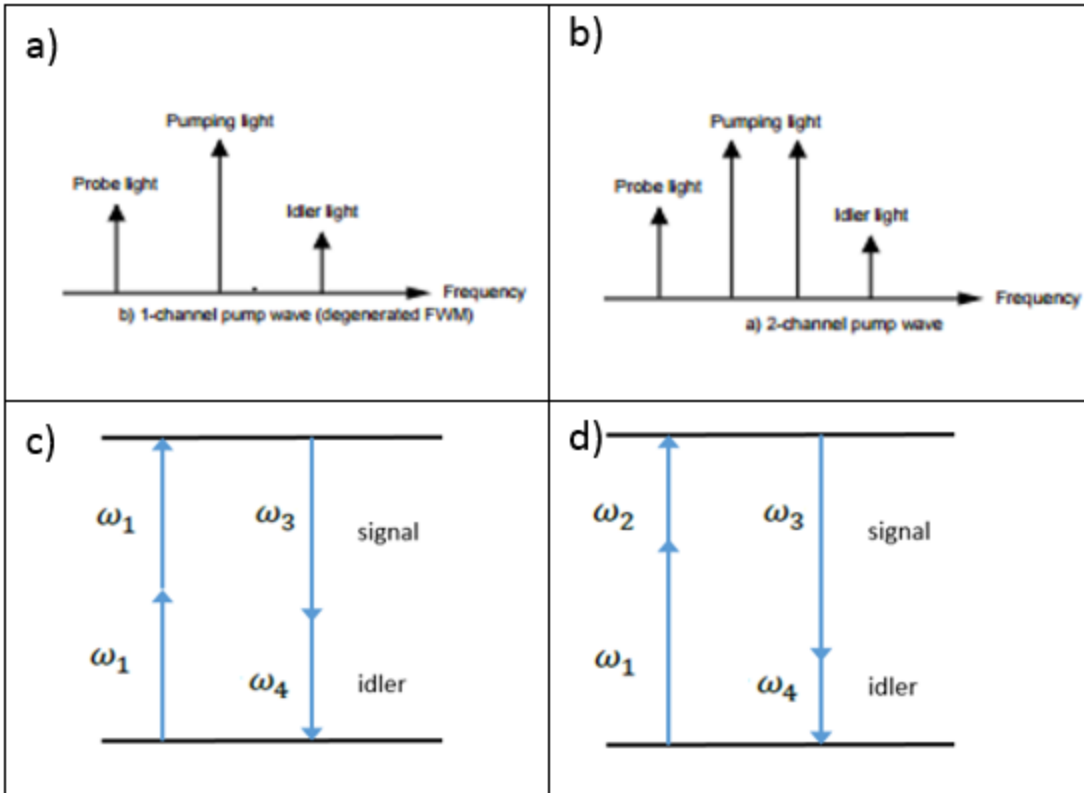


Figure 1.12 a) Degenerate FWM in the frequency domain b) Non-degenerate FWM in the frequency domain c) Degenerate FWM in an energy level diagram d) Non-degenerate FWM in an energy level diagram [22]

The main benefits of using a fiber optical parametric oscillator versus a bulk or solid state OPO are the alignment issues of the bulk, the size and weight, and the cost of constructing of each design.

1.7 Mode-Locked Laser Gyroscope

A technique that has been introduced into gyroscopes is the use of a mode-locked laser for the source instead of a continuous wave laser source. In this scenario, ultrashort pulse (ideally femtosecond second pulses) are counter propagated in the cavity resulting in the pulses interacting only a couple times in the cavity. This can be beneficial compared to the CW laser, because unlike the mode lock laser, the CW laser propagations interact with each other constantly. This can result in the previously stated lock-in effect when there is a low rotation rate [20]. The mode-locked laser gyro still follows the principles of the Sagnac theory, outputting overlapping pulse trains on a photodiode, resulting in a beat frequency.

In the mode-locked laser, there needs to be either an active element, such as an optical modulator, or nonlinear passive element, such as a saturable absorber. The latter of the two is what is being used for this project. In the active mode locking method, a modulator is inserted to the resonator to periodically modulate the phase change during the round trip [23]. When using active mode locking, the shortest pulses that can normally be achieved are in the picosecond range. The second method is passive mode locking. This technique uses a saturable absorber. This component normally has very high loss (In our case 80%), which is reduced at higher intensities. The saturable absorber modulates the resonator losses resulting in forming of ultrafast pulses. The duration of the pulses is dependent on the saturable absorbers recover time and the laser cavity design. Passive mode locking can produce pulses in the femtosecond range [24], [25].

Mode-Locking can be done in numerous types of laser designs. Some of those are; dye, bulk, and fiber. One of the first mode locked laser that was used for a gyroscope design was the dye laser. The dye used in the laser has a broad gain bandwidth, which is a standard requirement for mode locking. The dye lasers have some substantial disadvantages such as fast chemical degradation of the dye solution, and are limited in the amount of output power [26]. The solid-state laser has become the standard for mode-lock lasers, using a doped crystal or optic as the mode locking element. The solid state laser is very popular due to its ability to produce short pulses, stability, and a large range of output powers. In fiber lasers, high output power and pulse energy is more difficult to produce due to the higher nonlinear interaction, but an amplifier can be added on to the end of the laser without degradation of the pulse (with proper design). A particular fiber laser that has been designed is an all fiber bidirectional passive mode locked ring laser which produces two femtosecond pulse trains in counter directions. The use of a bidirectional laser can assist in the construction of a new and improved gyroscope [24]. If a bidirectional laser is not necessary, an isolator can be placed in the cavity to create a unidirectional laser. An issue with using a bidirectional laser is the order of components the pulse is seeing, if each fiber/component is not the correct length or acceptable, the two-outputting pulse may not be identical. The driving factor in obtaining lasing in both directions is the gain competition [24]. A way to eliminate the pulse interaction in the gain medium is to use an optical parametric oscillator. An OPO can be used because it has a very small 'excited state' lifetime. The gain is only present when there is a

pump pulse in the system. This results in an almost instantaneous reaction, removing the gain competition issue [20].

When moving from a CW laser to a mode locked laser, one might create a more stable source, but there are many more factors that have to be considered no matter the type of mode locked laser that is chosen. In these types of laser, the variables stated above cannot be changed independently, they all influence one another. A balance is needed in order to achieve a short pulse train, stability, and respectable efficiency.

2) Experimental Design

The drawing of the design of the entire system is shown in the figure below. Moving left to right, the first component is a pump source comprised of an all fiber Erbium doped mode locked laser working at a wavelength of 1560nm. The next stage is an Erbium doped fiber amplifier, used to increase the signal power coming out of the mode locked laser. In what follows is a grouping of couplers and output taps for monitoring and characterization purposes. This is significant in order to adjust the amount of power going into each arm of the OPO, and to monitor the output of each arm and the combined output. The final part is the actual fiber-based OPO ring in the design.

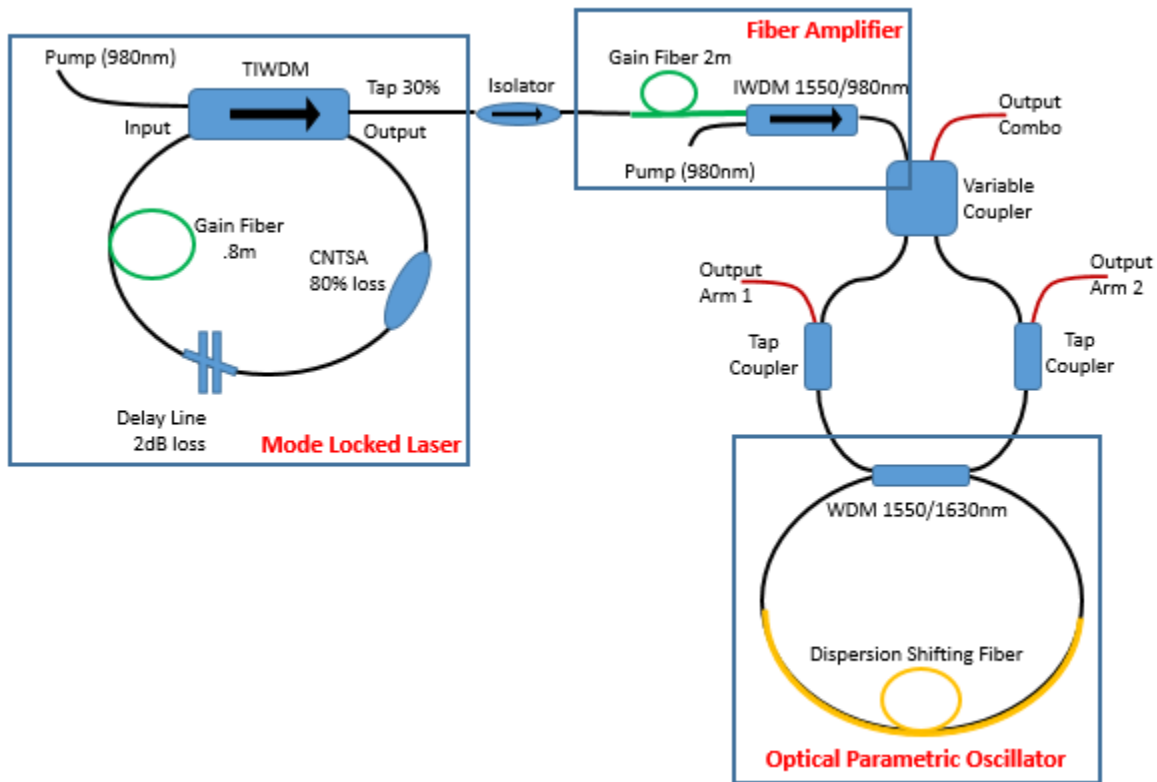


Figure 2.1 Schematic of the experiment consisting of the mode locked laser pump, fiber amplifier, and a bidirectional OPO

2.1 Mode Lock Laser Design

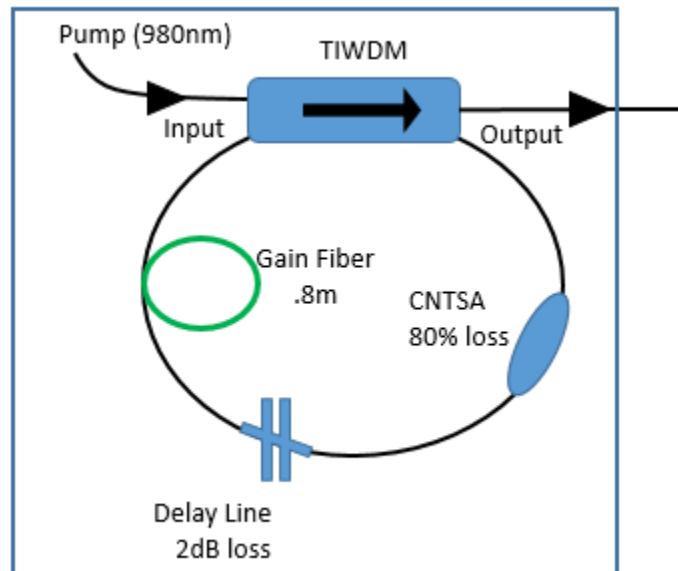


Figure 2.2 Schematic of Mode-Lock Fiber Laser

The source for this mode-locked laser is a diode pump laser working at 980 nm. The first component is a device that is a combination of a wave division multiplexer, an isolator, and an output coupler (a TIWDM hybrid device). By using a component that has all three functions in one package, it makes the whole laser more compact and minimizes the number of splices in the system, resulting in fewer losses, and less error. The WDM is necessary to launch the 980nm into the cavity, and for 1550nm to be used as a pump source for the rest of the experiment. The isolator in the TIWDM is used so the cavity is working only in a unidirectional fashion. Finally, the output coupler/Tap (30/70%) is used to extract the laser light out of the cavity into the next stage in the experiment. All the fiber that is being used in this mode-locked laser is polarizing maintaining fiber. The input channel is spliced to about 0.8 meters of erbium doped fiber that is used as the gain medium. The gain fiber goes into the delay line. This gives the degree of freedom to increase or decrease the cavity length so the cavity length of the mode locked laser and the fiber-based OPO downstream can be synced together. The final component in the laser is the carbon nanotube saturable absorber (CNTSA). This will be used as the mode-locking

portion of the laser [25]. The CNTSA is spliced back to the TIWDM at the output port to complete the ring laser cavity. The full characterization of all components of the laser and amplifier will be shown in the next section.

Measurements were taking on all the components for power loss and polarization performance. From using a known source, a polarization controller, and a power meter, it was determined that none of the components had issues/induced any polarization errors.

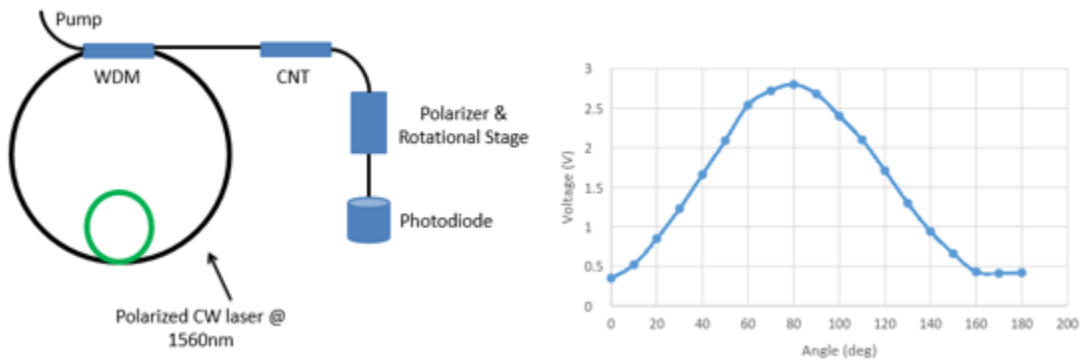


Figure 2.3 Setup for testing polarization, and the resulting voltage outputs

The general loss was found for each component. There was about 80% loss in the saturable absorber and about 2dB of loss in the delay line stage. The next figure shows the relationship between pump (980nm) current and the output laser power.

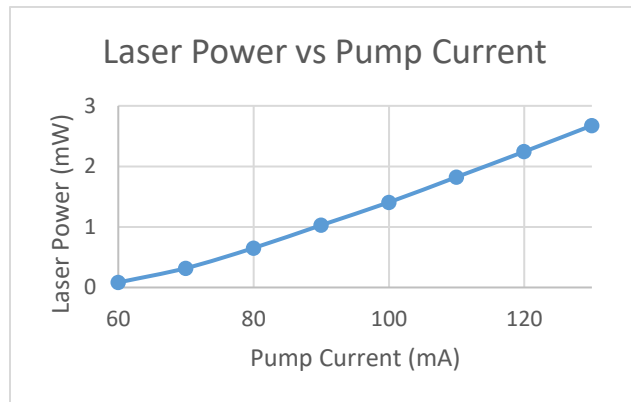


Figure 2.4 Mode-Locked Laser's output power

The laser began to mode lock at about 72mA and remained mode locked up to 100's of mA, but double pulsing (more than one pulse in the laser cavity) was seen at higher powers. It should be noted that at times during higher pumping the laser moved into the Q-switching regime. It was

determined that the laser should work at a lower pump power because of this and to ensure single pulsing mode and to minimize damage to the carbon nanotubes.

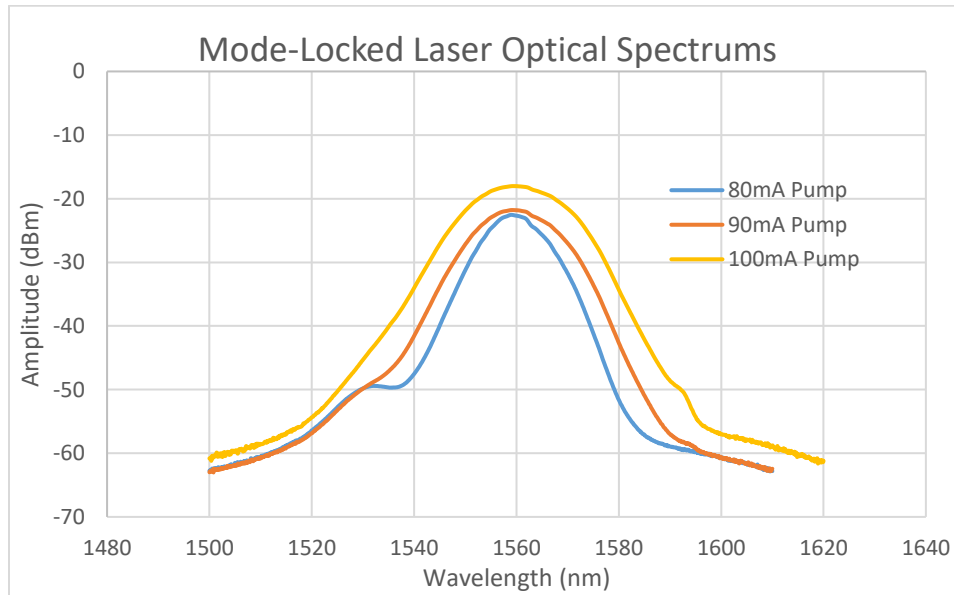


Figure 2.5 Multiple OSA readings for output spectrum of the Mode-Locked Laser

From looking at the plots above the 3 dB spectrum width is 10nm and approximately 21nm. By using the oscilloscope and the autocorrelator, the repetition rate and FWHM pulse width can be determined as 35.8MHz and 415fs respectively.

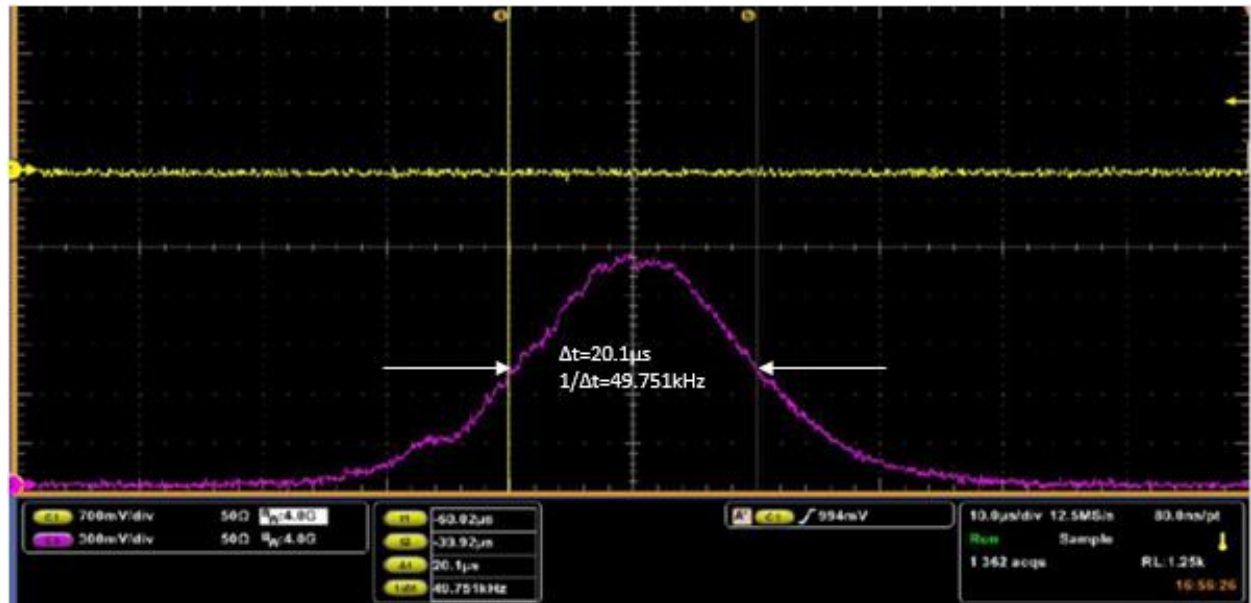
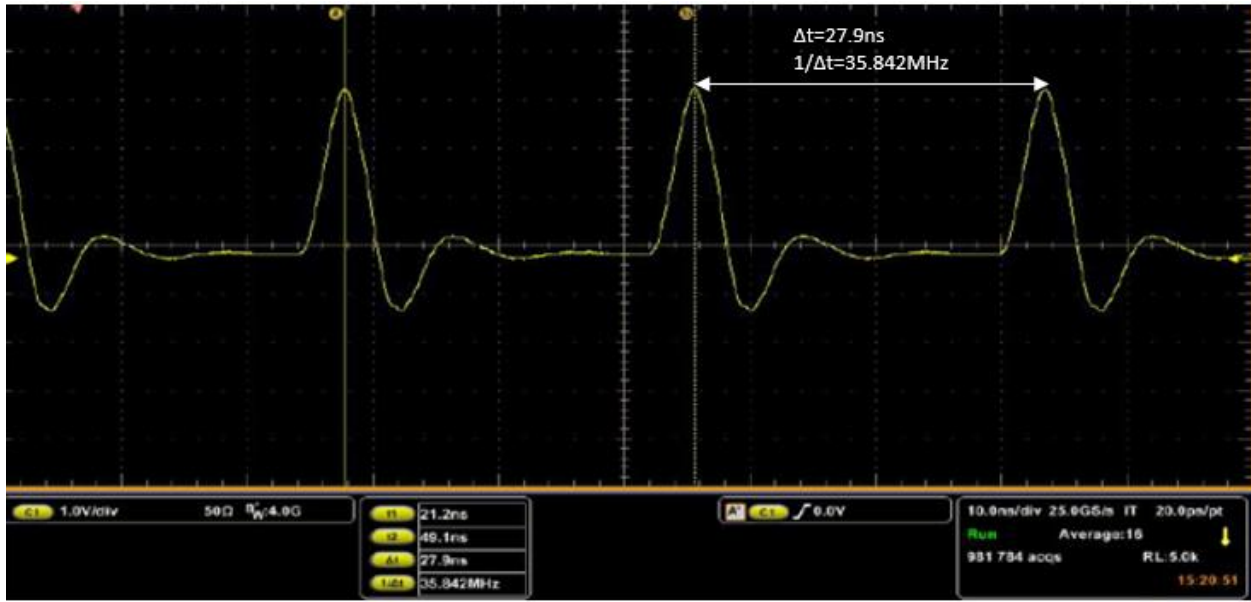


Figure 2.6 Top: Oscilloscope Reading Bottom: Autocorrelation of the Mode-Locked Laser

The output from the mode-lock laser is next spliced to another isolator so there is no back reflections or noise sent back to the mode locked laser cavity from another component that will be added later in the flow of the system. After the isolator, a homemade amplifier is placed in the structure.

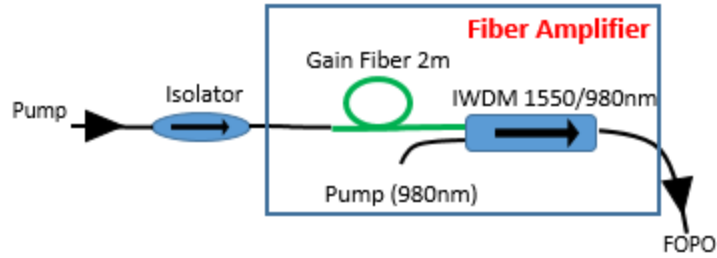


Figure 2.7 Isolator and Erbium Doped Fiber Amplifier

In past iterations of this setup a polarization controller would be next in line, but because of the polarization maintaining fiber being used, it is no longer needed in the current design [27]. This polarization maintaining erbium doped amplifier is comprised of an isolator WDM combination working at 980/1550nm, erbium doped gain fiber approximately 2 meters, and a 980nm pump. Just as the mode-locked laser is, the amplifier is made of all pm components. The characteristics of the laser after the amplifier will be shown below.

After the amplifier, the same tests were run to characterize the laser again, and to make sure it is running correctly.

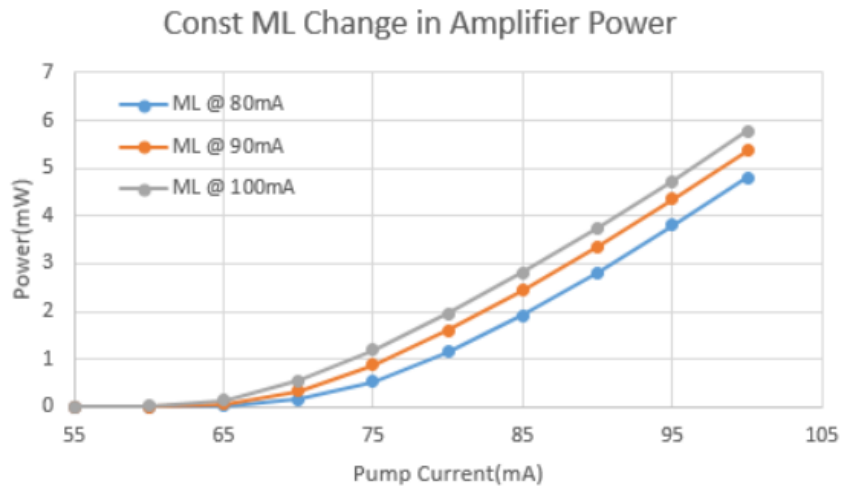


Figure 2.8 Output power after the amplifier. The pump current for the Mode-Locked laser remained constant while the pump for the amplifier was adjusted.

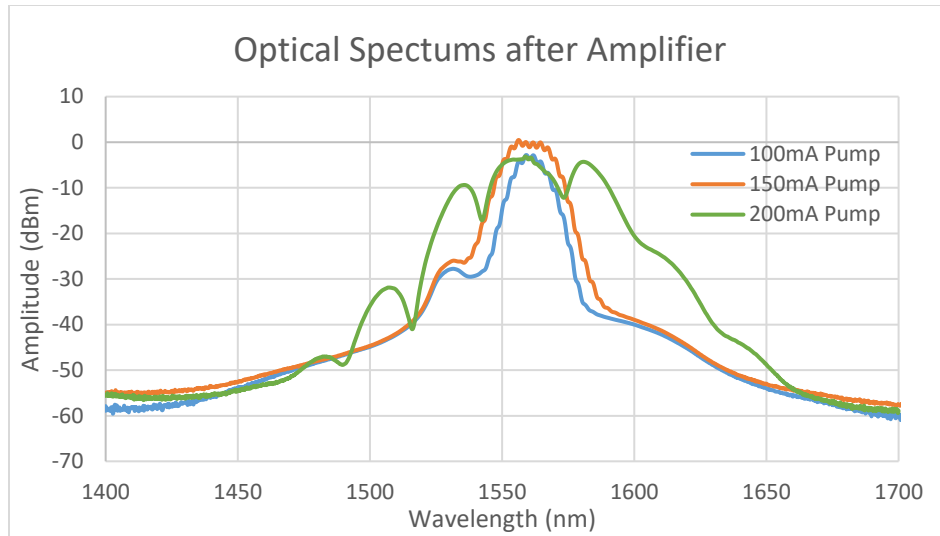


Figure 2.9 OSA readings after the amplifier

The spectra show that once the pump approaches a higher current it appears that the pulse is experiencing self-phase modulation (leading to significant spectral broadening), and eventually breaking. With using a pump current from 100 to 150mA the repetition rate remains at 35.84MHz, the spectrum width is still around 20nm, and the pulse width is approximately 280fs. Overtime the pumps for both the mode-locked laser and the amplifier had to be increased due excess loss in the system and the lifetime of the carbon nanotubes.

2.2 Bidirectional Fiber Optical Parametric Oscillator Design

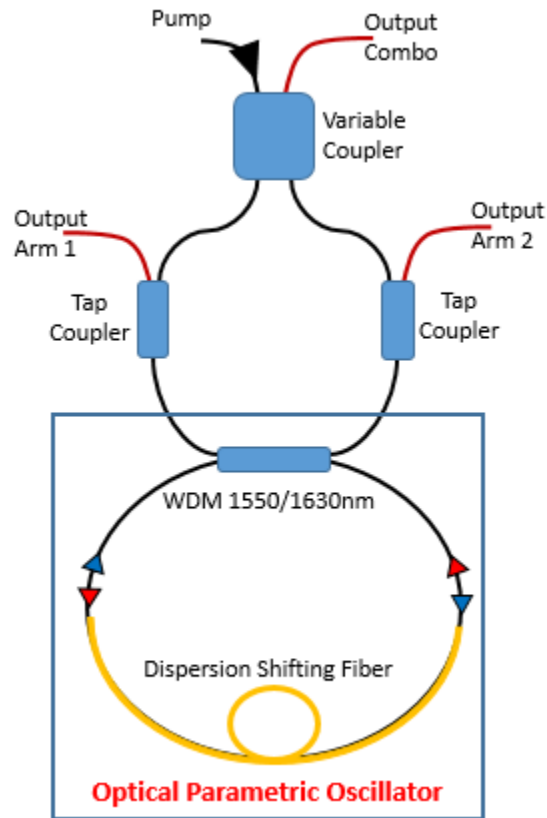


Figure 2.10 Couplers and Bidirectional Optical Parametric Oscillator

After the amplifier is the fiber-based OPO. There is a variable coupler that will determine the ratio of light that goes into each direction of the OPO. This will also be used to measure the output of the OPO when the counter propagating beams are recombined. Next are two tap couplers that are used to observe the signal generated from the OPO for both directions independently of one another. Finally, it is the actual OPO cavity which is made of a fused two by two WDM at 1560/1630. By using the two by two design this component can be used as an output coupler for both directions as well. Inside the cavity is a parametric gain fiber which is characterized as dispersion shifted fiber. There is about 5.5 meters of this fiber in the cavity with the rest of the fiber in the cavity being standard 1550nm pm fiber.

2.3 Housing Design

A housing was constructed for the experiment to try to mitigate environmental issues such as acoustics vibrations and thermal fluctuations. Two pieces of memory foam with each having the dimensions of 22in x 22in x 2in are used to cover the entire experiment. A channel was cut along the perimeter of the bottom piece of foam, about 2cm deep to place all the fiber, and in the middle of the bottom piece of foam divots were cut to place the bulkier pieces (the delay stage and the variable coupler). This was done so once the other piece of foam was placed on the top there will not be any extra stress or strain placed on the fiber. The fiber once laid in the channel looped around 2.5 times. A slit had to be cut through the middle of the foam in order to complete the loop. It is ideal to have setup laid out in one single loop for sensitivity purposes, but compared to the past iteration this design will have a larger sensing area. Also, if anything else is placed on the top of the foam it would not add extra stress as well. In the top piece of foam holes were cut in the same location as the divots for the delay stage and variable coupler so they can be adjusted without taking the entire top off, and disrupting the whole experiment. The foam that was cut for these holes can be inserted back to cover these components. A robust housing was designed to place this setup in. This housing is made up of aluminum t-slotted beams and polycarbonate panels, from 8020.org. This will hopefully help with the rest of the environmental variables that are present.

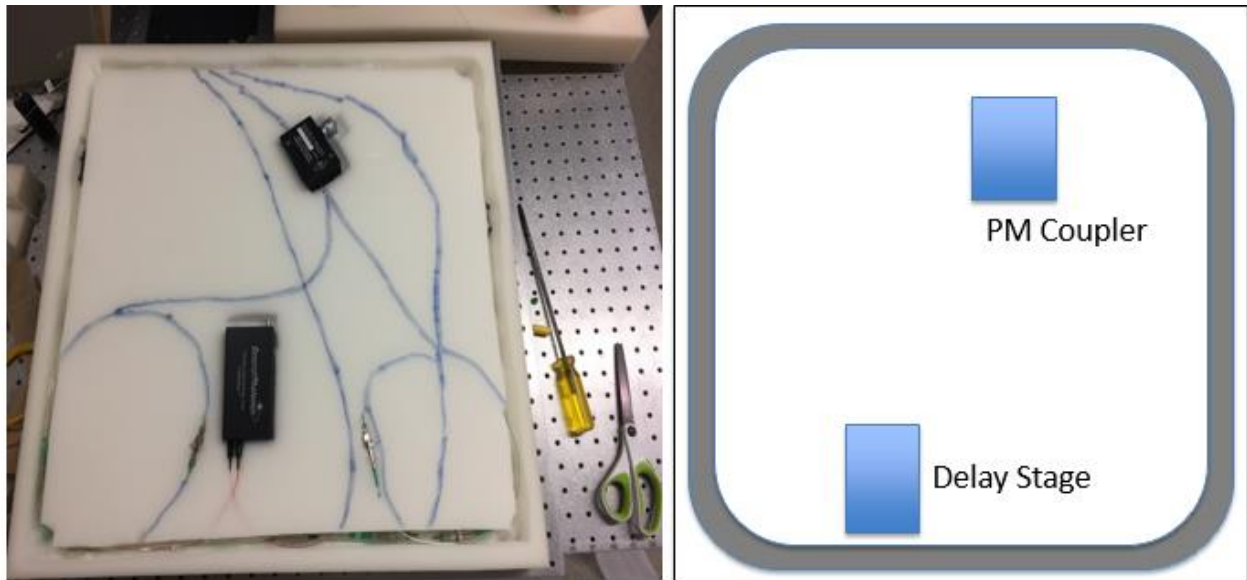


Figure 2.11 Layout in the bottom layer of foam

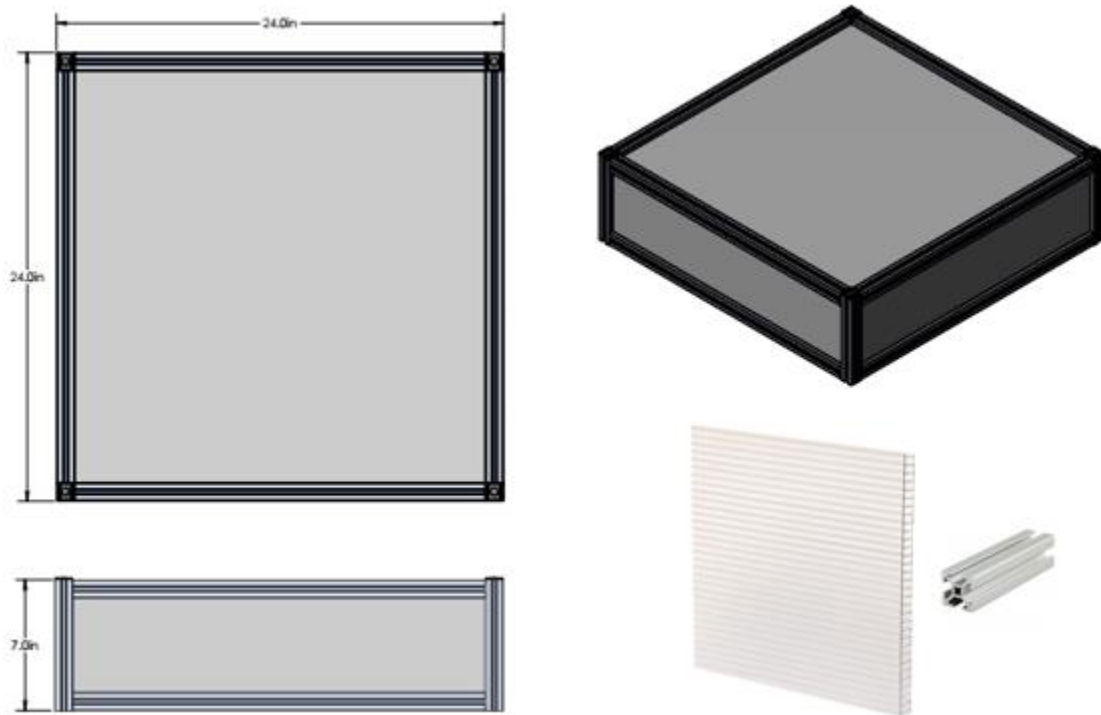


Figure 2.12 CAD drawing of the housing with the material components

By using this housing, it will give us the ability to also move the experiment from the current location to a different location, to collect measurements to identify if different environments are actually affecting the system. Such as the basement of the Meinel Building which could be

considered a location that has less temperature and acoustic fluctuations, and less of a natural mechanical oscillation.

3) Results

Once the variable coupler and delay line were adjusted to appropriate lengths and ratios, cavity synchronization can be achieved by observing the predicted wavelengths for the idler and signal on the optical spectrum analyzer, and by observing a beat signal on the RF spectrum analyzer. The cavities are synchronized when the cavity of the pump and the OPO are equal, having the same repetition rate. The optical spectrum analyzer was used first to observe the optical spectrums at the three output ports of the OPO. The two degrees of freedom were adjusted to first see the OPO lasing at the idler wavelength of the two individual arms at the same time. Then the combination arm was observed to view the appropriate optical spectrum. Once these have been fine-tuned, the setup becomes a turn-key system, i.e. once the pump is turned off and on the cavities automatically become synchronized.

A note about the mode-lock laser that was being used as the pump needed to be amplified over the length of the project. This was perhaps due to the lifetime of the carbon nanotubes in the cavity, and to the loss that was induced by the amount of spliced in the system, and perhaps some loss from using the polarization maintain fiber. At the point where this data was taken the 980 nm pump power was around 12-15mW. If it was anywhere above or below this region the laser would work as a Q-switch laser or would be double pulsing instead of the necessary mode-locked laser with a single laser pulse circulating around the laser cavity.

When looking at the optical spectrum the pump signal can be seen at around 1562nm and the idler can be seen at around 1646nm. These values are close to the expected wavelengths that were projected from the four-wave mixing phase matching condition (1560nm and 1620nm). The following figure shows the OPO spectrums.

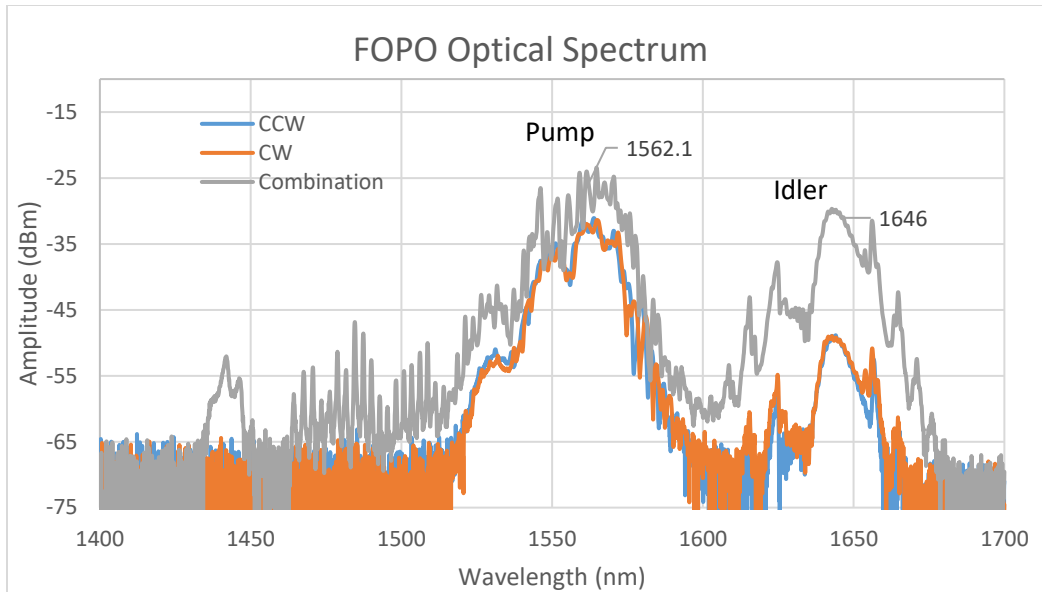


Figure 3.1 OSA reading for both arms and the recombined signal

From specifications for the FOPO that is being used the dispersion of the cavity is about 0.015ps^2 which falls under the anomalous region. For this region, the OPO is working in a standard soliton regime, and Kelly side bands can be detected.

Next the RF spectrum can be explained. A clear beatnote can be seen and proven due to the adjustment of the delay line in the pump cavity will shift the beat note. The reason for seeing this beatnote is the photodetector is detecting the carrier envelope offset for the two pulse trains that are generated in the cavity. This signal obviously cannot be seen in either individual arm. If the lengths of each arm are not equal, there can be a temporal delay (about $1.3\text{picoseconds/meter}$) with the pump and idler pulses. There is also a difference in the group velocity of the pulses as well. This issue is resolved by having the difference in lengths to be less than 10 centimeters. The fiber was measured out and this design met this requirement. Below is the RF spectrum reading for the combined output around the repetition rate, and a closer look at the beatnote with a slow detector.

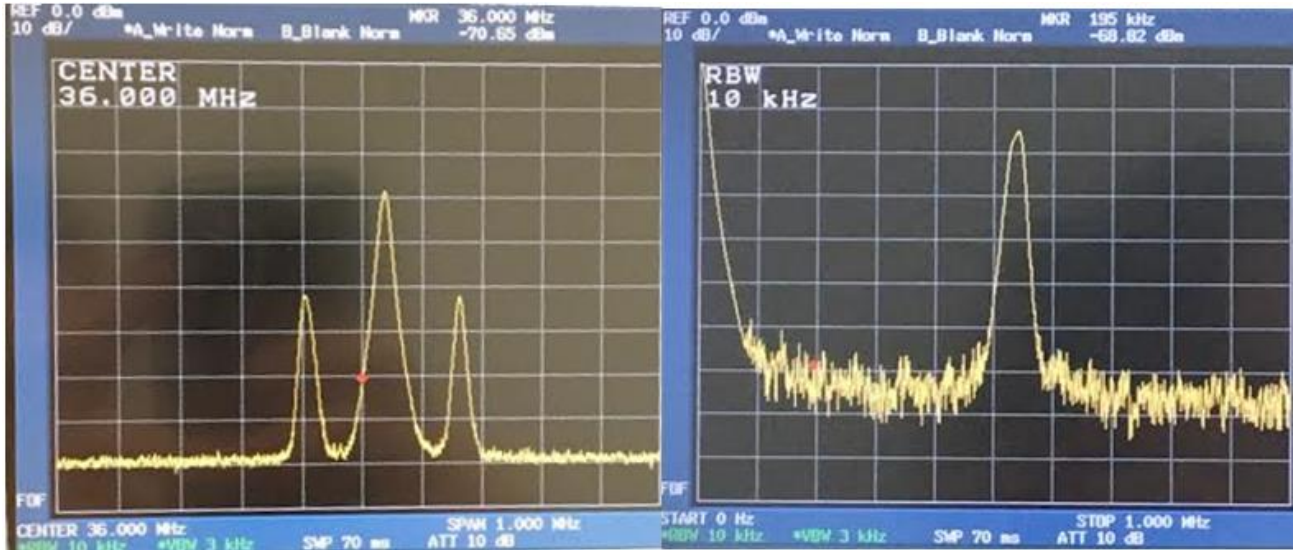


Figure 3.2 Left: shows the beatnote around the Repetition Rate. Right is a closer look at the beatnote signal

The beat signal can be shifted anywhere from less than 100 kHz to over 1 MHz. However, over a large amount of time when starting the signal at these ranges the beatnote can drift and become “lost” and adjustments need to be made to correct this issue. A linewidth of the beatnote was found to be approximately 300Hz. From observing this on the RF analyzer the linewidth is dependent on the resolution of the analyzer. Next the signal was observed with a slow photodiode on an oscilloscope. This will show the time depended signal, and the Fourier transform can be taken of this signal to find the corresponding frequency. The resulting bandwidth for this signal is approximately 45Hz.

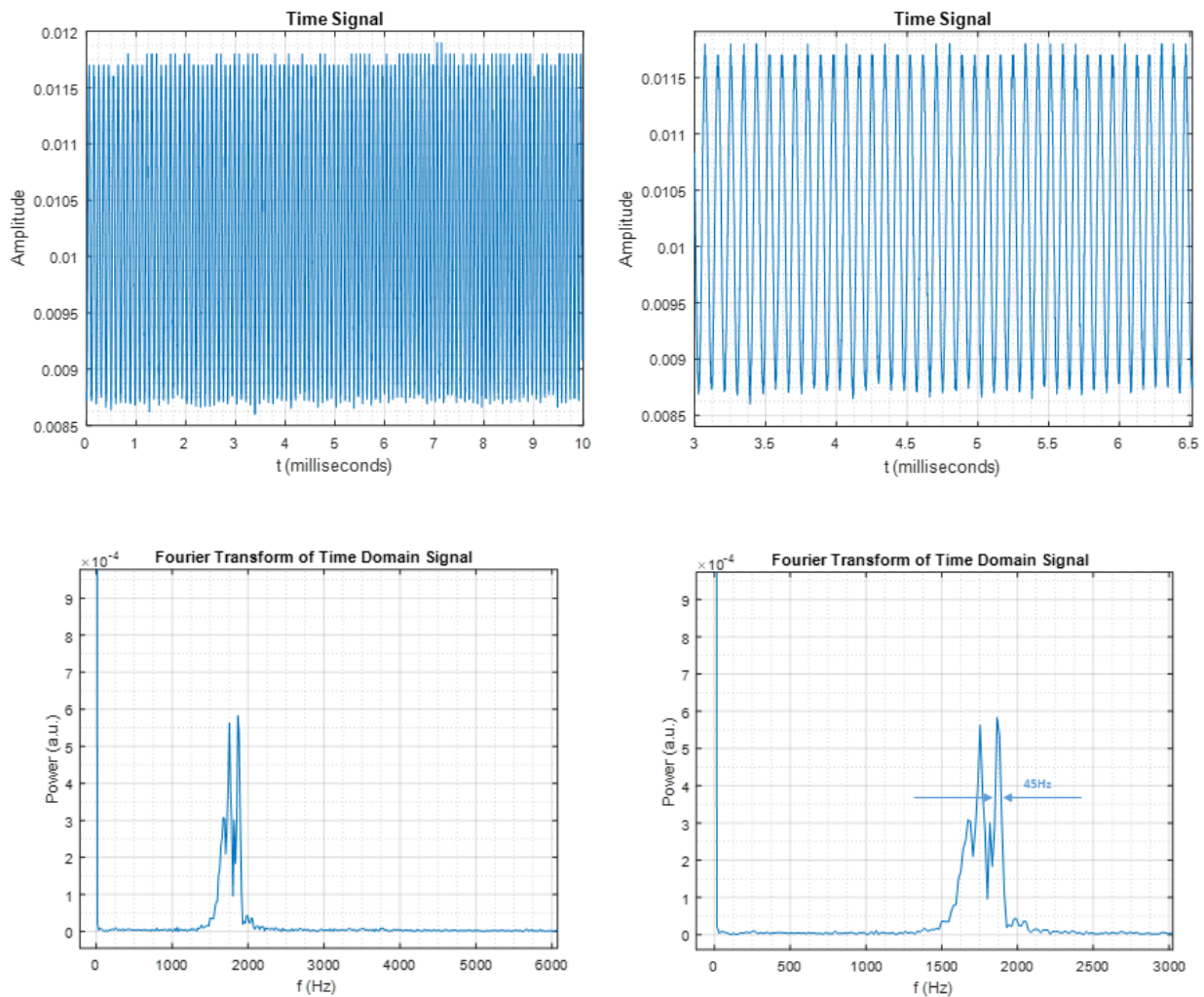


Figure 3.3 Time Signal and Fourier Transform

Now the drift issue is considered. Environmental factors were hypothesized as being the largest factor for the drift. As stated previously the design was sandwiched between two pieces of memory foam. To measure the drift the output was placed in a slow photodetector, and the detector was connected to a frequency counter. This was done for the design when it was inside and outside of the foam. The results of these measurements are shown in the following figure:

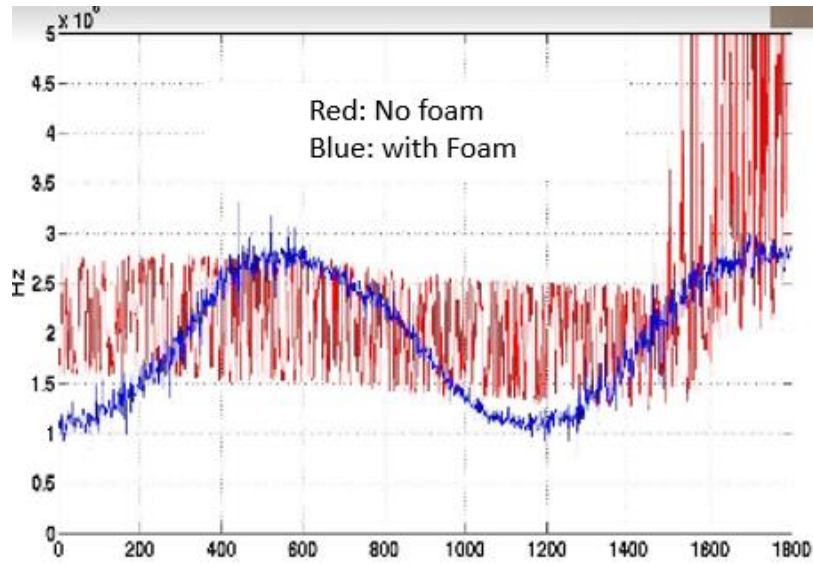


Figure 3.4 Frequency Counter readings with and without the foam

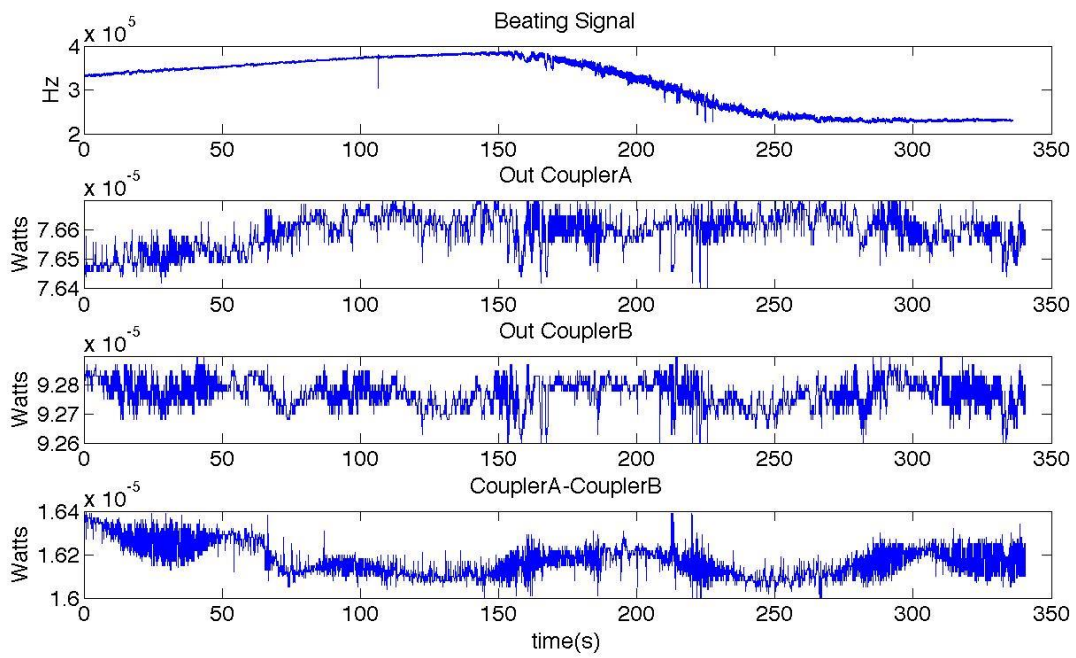


Figure 3.5 Power Readings from both arms

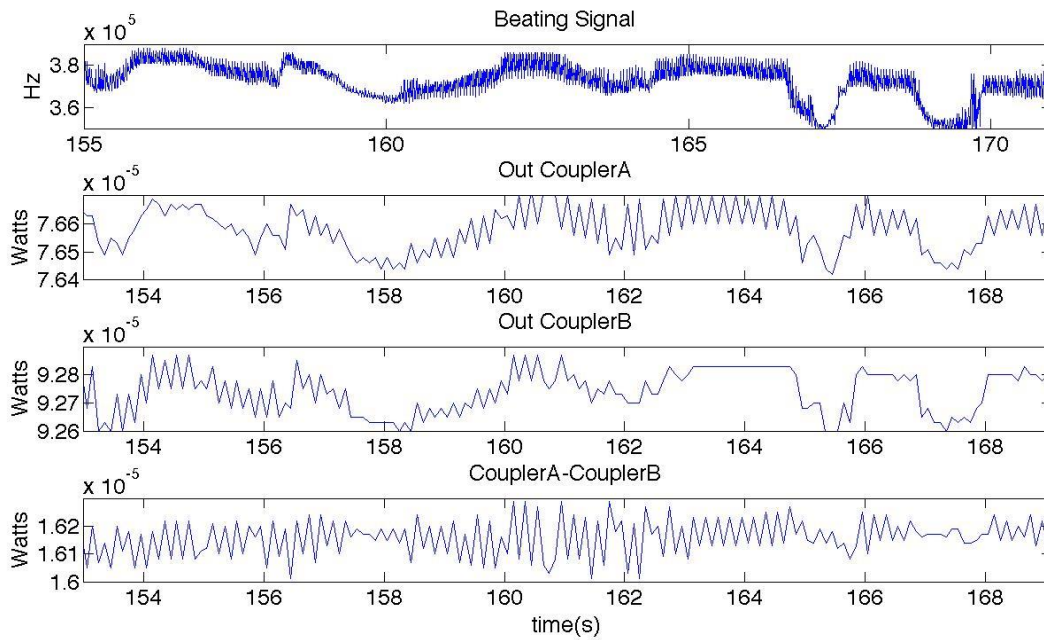


Figure 3.6 A zoomed in image of the power readings

The setup without the foam shows a large amount of movement over time, but once the setup is placed in the foam the frequency change slowed down to a slow sinusoidal trend. This change we believe is due to removing the acoustic effects on the design. Next the temperature fluctuation was looked at. Two temperature probes were placed in between the foam sheets, near the delay line and the variable coupler.

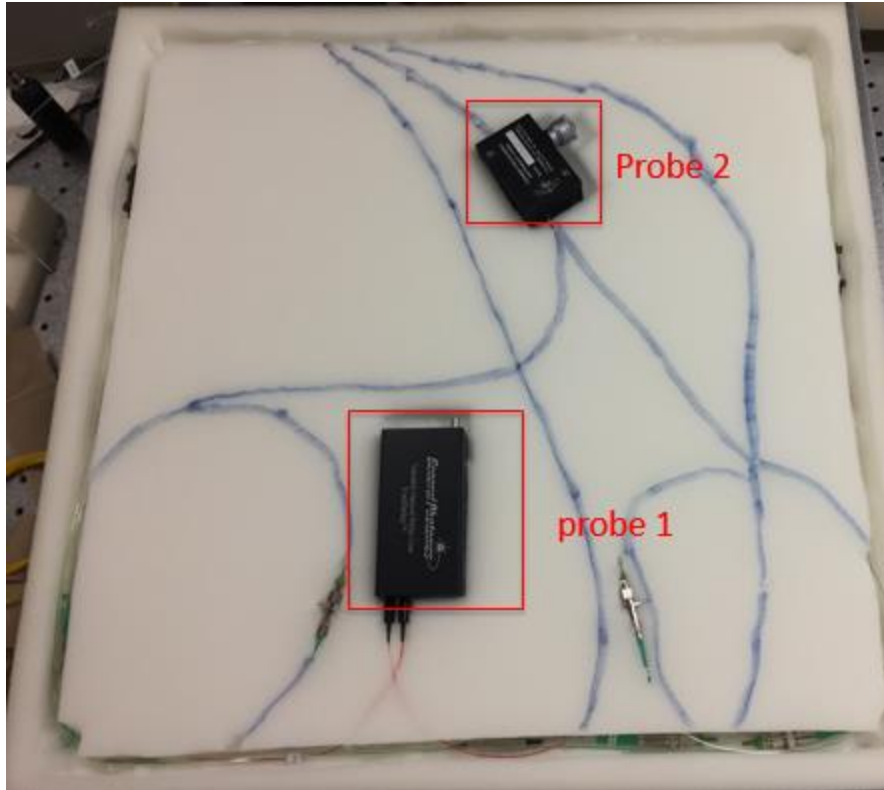


Figure 3.7 Shows the location of both the temperature probes in the system

The frequency counter test was run again while the temperature readings were being taken placed.

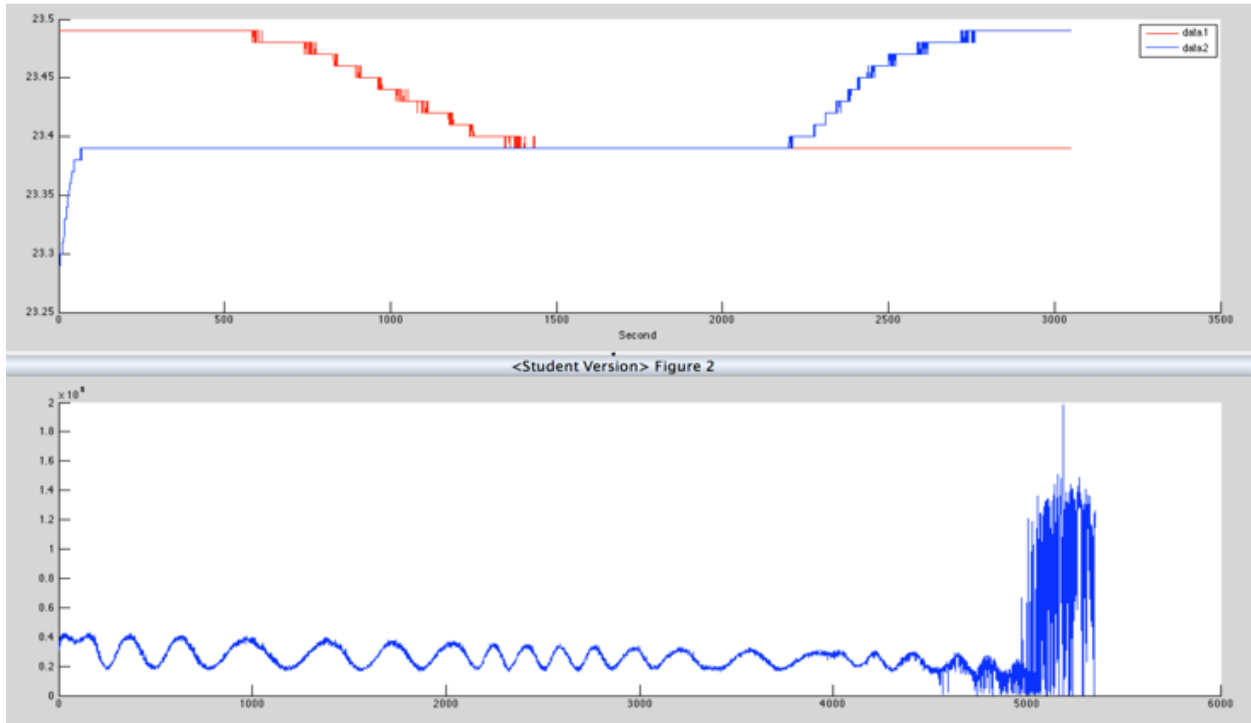


Figure 3.8 The relationship between temperature (top) and the frequency change/drift (bottom)

From looking at the plots for the temperature probes and the frequency counter, it appears that there is little to no correlation between temperature and frequency drift. The time domain signal of the drift measurements was taken and the Fourier transform was performed showing the drift frequency sensitivity.

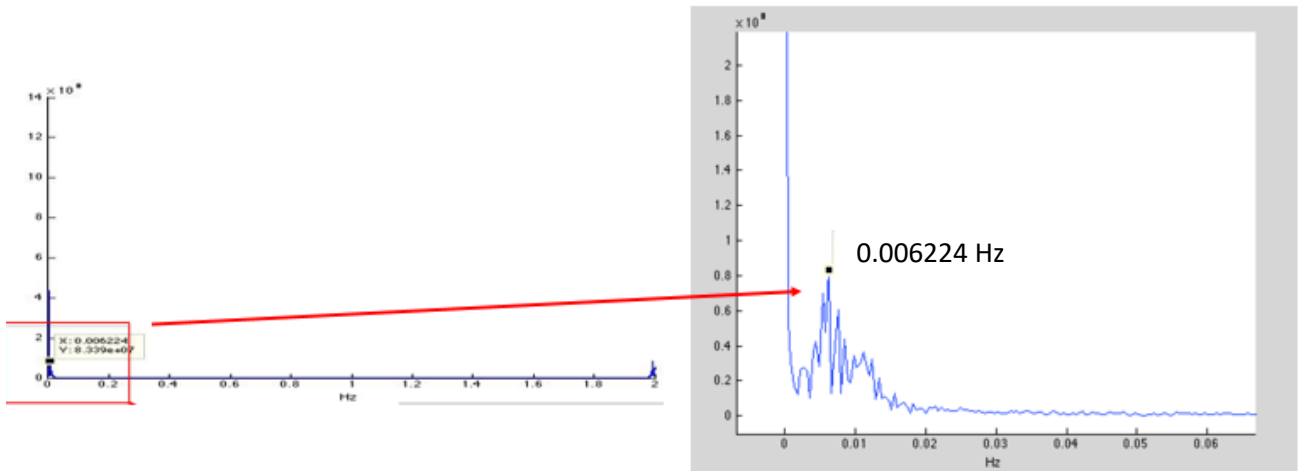


Figure 3.9 Fourier Transform of the drift measurements. Right is a zoomed in view of the left plot

At such a small frequency, it is still being evaluated on where this drift is coming from. A few theories are this is the natural oscillation of the building or one of the components in the setup, either delay line, or the variable coupler are not 100% stable. From crude calculations on building structure and rule of thumb building oscillations this appears to be a viable theory. As it is seen in the above plots over time the output begins to fluctuate rapidly, showing when the beatnote disappears, and the photodiode is reading random noise at this point. This tells us that over time the stabilization of the cavities still need to be addressed. This is being resolved by placing the whole design in an insulating box as stated before, and adding a fiber stretcher to the mode-locked laser for better stability. The noise that is being transferred from the pump to the OPO has been reduced by using the all pm mode-locked laser, but by adding the fiber stretcher piezo, and making this a fully stable frequency comb that noise can still be reduced further. Also, a stabilization mechanism can be added to the variable coupler to insure the power that is being split to both arms remains constant during the entire test run.

4) Conclusion

This report established an improved setup for a fiber optical parametric oscillator for gyro use. The fiber-based OPO is used as a Sagnac sensor system creating a beatnote at the output due to the carrier envelope offset of the two counter-propagating pulse trains. This system was built to work at a repetition rate of 35.8MHz. A more stable pump source was used (compared to previous experiments), consisting of all polarization maintain fiber/polarization maintain components including a specially design carbon nanotube saturable absorber, and a tap coupler, isolator, WDM combo piece to reduce splicing lose. Also by adding a foam housing to the design the drift in the beatnote was substantially reduced, and it was proven that temperature was not a significant variable in the amount of drift. This entire design has shown an improvement on previous setups for precise rotation measurements. By using an all fiber design, it should be noted that gyroscopes can be built with very high sensing areas that are considered robust and not as expensive as ring gyros or others that use bulk optics in their designs. There is still an issue with the drift over time, but for short times, i.e. hours/days the drift movement is manageable. Through techniques that were discussed it is believed that this design can be one of the most precise gyroscope designs constructed after optimization.

References

- [1] Anderson, R., H. R. Bilger, and G. E. Stedman. "'Sagnac' effect: A century of Earth-rotated interferometers." *American Journal of Physics* 62.11 (1994): 975-85. Web.
- [2] Bohn, Matthew John. *The Ti:sapphire ring laser gyroscope*. Thesis. 1998. N.p.: n.p., n.d. Print.
- [3] Stedman, G. E. "Ring-laser tests of fundamental physics and geophysics." *Reports on Progress in Physics* 60.6 (1997): 615-88. Web.
- [4] Rabeendran, Nishanthan. *A study of ring laser gyroscopes: a thesis submitted in partial fulfilment of the requirements for the degree of Master of Science, University of Canterbury*. Thesis. 2008. N.p.: n.p., n.d. Print
- [5] Macek, W. M., and D. T. M. Davis. "Rotation Rate Sensing With Traveling-Wave Ring Lasers." *Applied Physics Letters* 2.3 (1963): 67-68. Web.
- [6] Chow, W. W., J. Gea-Banacloche, L. M. Pedrotti, V. E. Sanders, W. Schleich, and M. O. Scully. "The ring laser gyro." *Reviews of Modern Physics* 57.1 (1985): 61-104. Web.
- [7] Juang Jeng-Nan, R. Radharamanan, "Evaluation of Ring Laser and Fiber Optic Gyroscope Technology", School Of Engineering Mercer University Macon GA, vol. 31207, 2009.
- [8] Lefèvre, Hervé. *The fiber-optic gyroscope*. Boston: Artech House, 1993. Print.
- [9] Ferrar, C.M., Progress in Fiber Optic Gyro Development, ISA Transactions, Vol. 28, No. 2, 1989.
- [10] Merlo, Sabina, and Silvano Donati. "Fiber Gyroscope Principles." *Handbook of Fibre Optic Sensing Technology*. Ed. Michele Norgian. 2000: John Wiley & Sons, n.d. 1-23. Print.
- [11] Shi, Chao-Xiang, and H. Kajioka. "A novel mode-locked fiber laser rotation sensor: Experiment." *Microwave and Optical Technology Letters* 12.4 (1996): 197-200. Web.
- [12] Kersey, A.D., Fiber Optic Gyroscope Technology, Optics News, November 1989, pp.12-19
- [13] Cvijetic, Milorad, and Ivan Djordjevic. *Advanced optical communication systems and networks*. Boston: Artech House, 2013. Print.

- [14] Schubert, E. Fred. *Light-emitting diodes, Chapter 22*. Cambridge, Uk: Cambridge U Press, 2003. 367-81 Print.
- [15] Boyd, Robert W. *Nonlinear optics, Chapter 9 Stimulated Brillouin and Stimulated Rayleigh Scattering*. San Diego, CA: Academic Press, 2003. 429-71. Print.
- [16] Boyd, Robert W. *Nonlinear optics, Chapter 10 Stimulated Raman Scattering and Stimulated Rayleigh-Wing Scattering*. San Diego, CA: Academic Press, 2003. 473-509. Print.
- [17] Fujii, Yoichi, and Koichi Sanos. "Polarization transmission characteristics of optical fibers with elliptical cross section." *Electronics and Communications in Japan (Part I: Communications)* 63.8 (1980): 87-93. Web.
- [18] Carter, Adrian; Samson, Bryce "PANDA-style fibers move beyond telecom". *Laser Focus World*. (August 2004).Web.
- [19] Zlobina, E. A., and S. I. Kablukov. "Fiber optical parametric oscillators." *Optoelectronics, Instrumentation and Data Processing* 49.4 (2013): 363-82. Web.
- [20] Meng, Xianmei, Jean-Claude Diels, Dietrich Kuehlke, Robert Batchko, and Robert Byer. "Bidirectional, synchronously pumped, ring optical parametric oscillator." *Optics Letters* 26.5 (2001): 265. Web.
- [21] Nguyen, T. N., K. Kieu, A. V. Maslov, M. Miyawaki, and N. Peyghambarian. "Normal dispersion femtosecond fiber optical parametric oscillator." *Optics Letters* 38.18 (2013): 3616. Web.
- [22] Aso, Osamu, Masateru Tadakuma, and Shu Namiki. "Four-Wave Mixing in Optical Fibers and Its Applications." *Furukawa Review* 19. (2000) Web
- [23] Jeon, M. Y., H. J. Jeong, and B. Y. Kim. "Mode-locked fiber laser gyroscope." *Optics Letters* 18.4 (1993): 320. Web.
- [24] Kieu, Khanh, and Masud Mansuripur. "All-fiber bidirectional passively mode-locked ring laser." *Optics Letters* 33.1 (2007): 64. Web.
- [25] Kieu, Khanh, and Masud Mansuripur. "Femtosecond laser pulse generation with a fiber taper embedded in carbon nanotube/polymer composite." *Optics Letters* 32.15 (2007): 2242. Web.
- [26] Dennis, Michael L., Jean-Claude M. Diels, and Ming Lai. "Femtosecond ring dye laser: a potential new laser gyro." *Optics Letters* 16.7 (1991): 529. Web.

- [27] Gowda, Roopa, Nam Nguyen, Jean-Claude Diels, Robert Norwood, Nasser Peyghambarian, and Khanh Q. Kieu. "All-fiber bidirectional optical parametric oscillator for precision rotation sensing." *Cleo: 2015* (2015): n. pag. Web.